

Auger decay of degenerate and Bose-condensed excitons in Cu₂O

G. M. Kavoulakis and Gordon Baym

Department of Physics, University of Illinois at Urbana-Champaign, 1110 West Green Street, Urbana, Illinois 61801

(Received 16 February 1996; revised manuscript received 28 June 1996)

We study the nonradiative Auger decay of excitons in Cu₂O, in which two excitons scatter to an excited electron and hole. The exciton decay rate for the direct and the phonon-assisted processes is calculated from first principles; incorporating the band structure of the material leads to a relatively shorter lifetime of the triplet-state ortho excitons. We compare our results with the Auger decay rate extracted from data on highly degenerate triplet excitons and Bose-condensed singlet excitons in Cu₂O. [S0163-1829(96)00346-3]

I. INTRODUCTION

Recent experiments on excitons in Cu₂O have been carried out at sufficiently high densities and low enough temperatures that the Bose-Einstein statistics they obey becomes significant,¹ and, indeed, in stressed samples, Bose-Einstein condensation of excitons has been observed. As we have shown in Ref. 2, the crucial barrier to condensing excitons is heating of the exciton gas by the nonradiative *Auger decay* process, in which two excitons collide to produce an ionized electron and hole. See Fig. 1. This process not only heats the gas, but it leads to loss of excitons as well. (The Auger process is familiar in electron-hole plasmas, in which the recombination of an electron and a hole excites either an electron high in the conduction band or a hole deep in the valence band. This process has been studied there both theoretically³ and experimentally.⁴) In this paper we present detailed calculations of the Auger process in Cu₂O that we used in Ref. 2 to calculate the time evolution of the exciton gas in Cu₂O following laser excitation. Other exciton-exciton scattering processes that can play a similar role to the Auger process are suppressed thermally; for example, the process of two excitons colliding giving an exciton and an electron-hole pair in the final states requires at least one exciton to have a thermal energy on the order of the exciton binding energy. Therefore a negligible number of excitons can participate in this process.

In the Cu₂O experiments, intense pulses of laser light excite the crystal, creating a gas of (triplet) ortho excitons and (singlet) para excitons, split by an exchange energy $\Delta E \approx 12$ meV.⁵ We note that band-gap renormalization effects caused by the excited excitons are not expected to be significant in Cu₂O since the dimensionless quantity na_B^3 is on the order of 10^{-3} for the highest densities, where n is the density of excitons and $a_B \approx 5.3 \text{ \AA}$ is the exciton Bohr radius; a situation in contrast to other semiconductors in which the Bohr radius is much larger. We know of no experimental evidence for such band-gap renormalization in Cu₂O, even at the highest densities. The kinetic energy distribution of ortho excitons as a function of time from the onset of the laser pulse is observed by spectroscopy of their photoluminescence (considerably more intense than that of the para excitons). In the classical (low-density) regime, the energy

distribution is observed to be Maxwell-Boltzmann, described by an effective exciton temperature. In the quantum (high-density) regime, the spectra are well fit in terms of an ideal Bose-Einstein gas with an instantaneous chemical potential, μ , and temperature, T . From these parameters, one can directly calculate the density of the gas. The experiments of Snoke *et al.* observe a “quantum saturation” of the ortho excitons, i.e., a tendency for them to move closely parallel to the critical line without condensing.¹ The critical line, an adiabat (constant entropy per particle, $s = S/N$), has the form, $T_c = (2\pi\hbar^2/mk_B)[n/g\zeta(3/2)]^{2/3}$, where the degeneracy $g = 3$ for ortho excitons and 1 for para excitons. In general lines in the phase diagram parallel (in a log-log plot) to the condensation line at higher temperature are adiabats.

The important role of the Auger process has been revealed in several experiments. The inverse of the total decay time of ortho excitons in Cu₂O shows an approximate proportionality to their density; the data for nonstressed

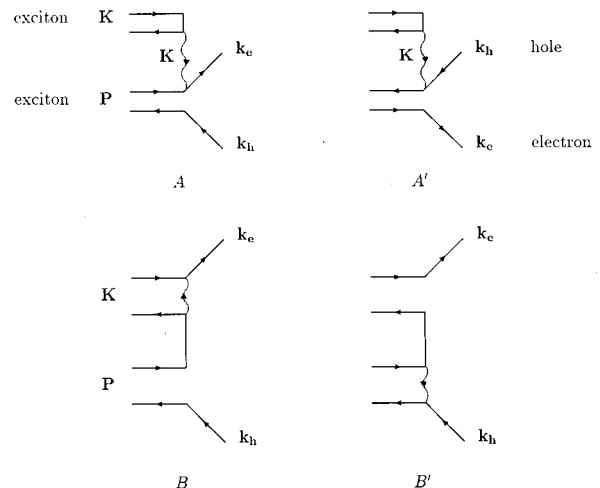


FIG. 1. Two classes of diagrams for the direct Auger nonradiative recombination. Time progresses from left to right. The initial state contains two excitons of momenta \mathbf{K} and \mathbf{P} , and the final state contains an ionized electron and hole with momenta \mathbf{k}_e and \mathbf{k}_h , respectively. The dashed line denotes the Coulomb interaction. Processes A and A' are the dominant ones and they are nonzero only if the recombined particle is an ortho exciton.

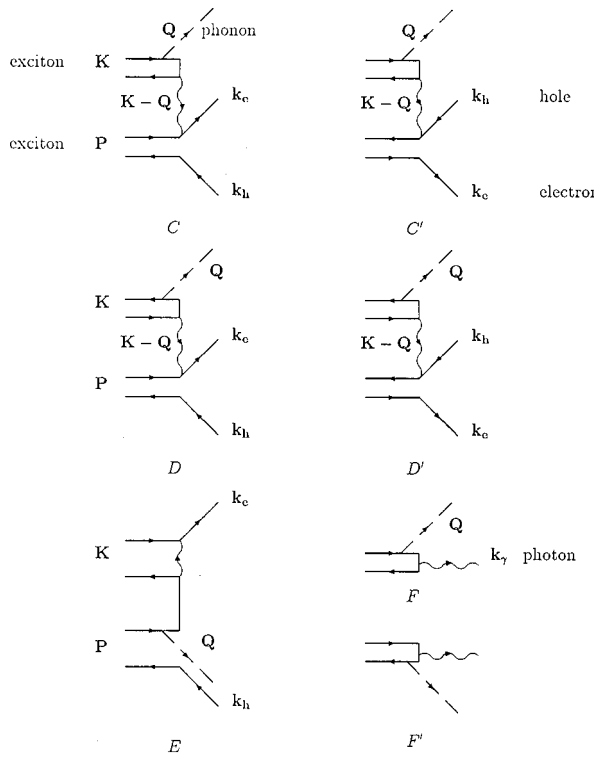


FIG. 2. The phonon-assisted Auger process (diagrams C , C' , D , D' , and E), and the phonon-assisted radiative recombination process (F and F'). The phonon is denoted by a dashed line. Processes D and D' are the dominant ones because of the band structure of Cu_2O . In these, the recombined exciton can only be an ortho exciton. Similarly, diagram F is dominant compared to F' ; the recombined exciton can only be an ortho exciton.

crystals^{6,7} is shown in Fig. 6 of Ref. 7. In this figure the quotes indicate that the density plotted on the horizontal axis is assumed to be proportional to the total radiative recombination luminescence intensity and is calibrated by comparison to the density deduced from spectral fits. The total decay rate is a sum of interconversion of ortho excitons into para excitons⁸ and the Auger process; the rates of both processes are comparable. An additional feature of the Auger process is that it leads to a much shorter lifetime of ortho excitons; in lightly stressed crystals the observed ortho-exciton decay time is ~ 0.1 ns (Ref. 9) compared with the para-exciton lifetime at high para-exciton density, $\sim 10^{19}$ cm^{-3} , which exceeds 100 ns. The Auger process also leads to the presence of ortho excitons in quantum wells, caused by high stress, for times much longer than the ortho-exciton lifetime; although the exciton gas in the wells consists primarily of para excitons, high-energy electrons and holes produced in Auger ionization of para excitons lead to reformation of excitons in essentially random internal angular momentum states.¹⁰

Here we calculate the Auger decay rate for both the direct and phonon-assisted mechanisms, Figs. 1 and 2. One of our basic conclusions is that the rate of the phonon-assisted Auger mechanism is much larger than the rate of the direct process, a consequence of the conduction and the valence bands having the same parity. Although the phonon-assisted mechanism requires participation of a phonon, the rate is

enhanced because the process is dipole allowed. In Sec. II, we first derive the matrix element of the direct Auger process, neglecting for simplicity at this stage the angular momentum structure of the excitons, then we discuss detailed approximations to the matrix element and calculate the decay rate for the direct process. In Sec. III we generalize the results to take into account the full angular momentum structure of the ortho and para excitons in Cu_2O and explain how specific properties of the excitons in this material are related to the direct Auger process. We then turn, in Sec. IV, to consider the phonon-assisted Auger process and discuss its connection with the phonon-assisted radiative recombination of excitons in Cu_2O . In Sec. V, we take into account the effects of the Pauli principle on the decay rate. Finally, in Sec. VI, we compare our results with the measured rate and summarize our conclusions.

II. DIRECT PROCESS — CALCULATION OF THE MATRIX ELEMENT AND THE DECAY RATE

The direct Auger process is described by the sum of the topologically distinct Feynman diagrams shown in Fig. 1. In this figure, time progresses from left to right; the solid lines with forward-going arrows denote electrons, and those with backward-going arrows denote holes. The initial state contains two excitons, of center-of-mass momenta \mathbf{K} and \mathbf{P} , described by the wave function

$$\Psi_i = \Psi_{\mathbf{K}}(\mathbf{x}_e, \mathbf{x}_h) \Psi_{\mathbf{P}}(\mathbf{x}'_e, \mathbf{x}'_h), \quad (1)$$

where $\Psi_{\mathbf{Q}}$ denotes the full wave function of an exciton of total momentum \mathbf{Q} , and the \mathbf{x}_i denote electron and hole coordinates. We include effects of symmetrization below. The final state contains an ionized electron of momentum \mathbf{k}_e and an ionized hole of momentum \mathbf{k}_h , described by the wave function

$$\Psi_f = \Phi_{c, \mathbf{k}_e}(\mathbf{x}_e) \Phi_{v, \mathbf{k}_h}(\mathbf{x}_h), \quad (2)$$

where the $\Phi_{j, \mathbf{k}}(\mathbf{x})$ are the normalized Bloch wave functions for the ionized electron and hole in the final state, and the subscripts c, v denote the conduction and valence bands. The wiggly line in the figure denotes the screened Coulomb interaction. In the first class of diagrams, A and A' , the electron and hole in the same exciton recombine; in the second class, B and B' , particles of different excitons recombine.

The exciton wave functions $\Psi_{\mathbf{Q}}(\mathbf{x}_e, \mathbf{x}_h)$ can be expressed in terms of the electron and hole Bloch wave functions as

$$\Psi_{\mathbf{Q}}(\mathbf{x}_e, \mathbf{x}_h) = \sum_{\mathbf{q}} \phi_{\mathbf{q}} \Phi_{c, \mathbf{q}+\mathbf{Q}/2}(\mathbf{x}_e) \Phi_{v, -\mathbf{q}+\mathbf{Q}/2}(\mathbf{x}_h), \quad (3)$$

where the Bloch wave functions $\Phi_{j, \mathbf{k}}(\mathbf{x})$ in band j are

$$\Phi_{j, \mathbf{k}}(\mathbf{x}) = u_{j, \mathbf{k}}(\mathbf{x}) e^{i\mathbf{k} \cdot \mathbf{x}}. \quad (4)$$

The momentum \mathbf{q} in the $\Phi_{i, \mathbf{q}}$ in Eq. (3) is restricted to be inside the first Brillouin zone. In general the sum on the right of this equation should include all the conduction and valence bands, but for simplicity we neglect all other bands except the lowest conduction and the highest valence, which

is a rather good approximation for the case of Cu_2O . In the effective-mass approximation for the exciton wave function, with equal electron and hole effective masses $\Psi_{\mathbf{Q}}$ takes the form

$$\Psi_{\mathbf{Q}}(\mathbf{x}_e, \mathbf{x}_h) = \frac{1}{\sqrt{\Omega}} e^{i\mathbf{Q} \cdot (\mathbf{x}_e + \mathbf{x}_h)/2} \phi_{\text{rel}}(\mathbf{x}_e - \mathbf{x}_h), \quad (5)$$

where Ω is the crystal volume, and ϕ_{rel} is the relative electron-hole wave function. Comparing Eqs. (3) and (5) we see that $\phi_{\mathbf{q}}$ is the Fourier transform of ϕ_{rel} times $\sqrt{\Omega}$; to a good approximation, we may make this identification even when using complete Bloch waves, Eq. (4).

The interaction between the excitons is, in general, the dynamically screened Coulomb interaction, $V_{\text{eff}}(\mathbf{k}, \omega) = V_{\text{Coulomb}}(\mathbf{k})/\epsilon(\mathbf{k}, \omega)$, where the dielectric function is given by the usual Lindhard result

$$\epsilon(\mathbf{k}, \omega) = \epsilon_{\infty} - V_{\text{Coulomb}}(\mathbf{k}) \sum_{q, l, l'} \frac{n_{l', \mathbf{k}+\mathbf{q}} - n_{l, \mathbf{q}}}{\epsilon_{l', \mathbf{k}+\mathbf{q}} - \epsilon_{l, \mathbf{q}} - \hbar\omega} \times |\langle u_{l', \mathbf{k}+\mathbf{q}} | u_{l, \mathbf{q}} \rangle|^2, \quad (6)$$

with ϵ_{∞} the high-frequency dielectric constant of the material, and l and l' band indices. The second term in Eq. (6) can in fact be neglected in the Auger process, where we are interested primarily in small momentum transfers of order the thermal momentum of excitons, $P^2/2M_{\text{exc}}$ on the scale of 1–10 meV, but rather large frequencies corresponding to energy transfer on the order of the energy gap, $\hbar\omega \approx E_g = 2.17$ eV. In this limit, the terms in Eq. (6) involving the same band vanish for finite ω . In the same limit, for different bands, $l \neq l'$, the sum in Eq. (6) is proportional to k^2 for small momenta, from the overlap integral between different bands, due to the orthogonality of the Bloch functions. This factor of k^2 cancels with the $1/k^2$ from the Coulomb potential and therefore the last term on the right side of Eq. (6) is k independent and is in fact rather small for the densities of interest. More precisely, an estimate¹¹ of the overlap integral in Eq. (6) is $\hbar^2 k^2 / 2m(E_g + \Delta)$, where Δ is the energy difference between the lowest Γ_7^+ conduction band and the higher Γ_8^- band and m is the bare-electron mass. Thus, an upper bound of the second term on the right side of Eq. (6) is $(\hbar\omega_p)^2 / 2(E_g + \Delta)\Delta$, where ω_p is the plasma frequency and Δ is the energy difference between the lowest Γ_7^+ conduction band and the higher Γ_8^- band. Since the plasma frequency in optically excited semiconductors is much smaller than the energy splitting of the bands, this term is smaller than 10^{-2} . Thus, $\epsilon(\mathbf{k}, \omega_g) \approx \epsilon_{\infty}$, and the effective interaction, essentially independent of ω for large ω , becomes

$$V_{\text{eff}}(\mathbf{k}) = \frac{4\pi e^2}{\Omega \epsilon_{\infty} k^2}. \quad (7)$$

We note that as a consequence of Cu_2O being almost nonpolar,¹² $\epsilon_{\infty} (\approx 6.46)$ and the static dielectric constant $\epsilon_0 (\approx 7.5)$ differ only slightly.

Assembling these results, we find that the matrix element $M \equiv \langle \Psi_f | V | \Psi_i \rangle$ between the initial and final states, for diagram A for example, is thus

$$M_A = \sum_{\mathbf{q}, \mathbf{G}, \mathbf{G}'} \phi_{-\mathbf{k}_h + \mathbf{P}/2} V_{\text{eff}}(\mathbf{G} - \mathbf{K}) \phi_{\mathbf{q}} \langle u_{v, \mathbf{q} - \mathbf{K}/2} | u_{c, \mathbf{q} + \mathbf{K}/2} \rangle_{\mathbf{G}} \times \langle u_{c, \mathbf{k}_e} | u_{c, \mathbf{k}_e + \mathbf{K}} \rangle_{\mathbf{G}'} \delta_{\mathbf{k}_e + \mathbf{k}_h + \mathbf{G} + \mathbf{G}', \mathbf{K} + \mathbf{P}}, \quad (8)$$

where

$$\langle u_{v, \mathbf{q} - \mathbf{K}/2} | u_{c, \mathbf{q} + \mathbf{K}/2} \rangle_{\mathbf{G}} \equiv \int d\mathbf{x} u_{v, \mathbf{q} - \mathbf{K}/2}^*(\mathbf{x}) u_{c, \mathbf{q} + \mathbf{K}/2}(\mathbf{x}) e^{i\mathbf{G} \cdot \mathbf{x}} \quad (9)$$

is a generalized overlap integral¹³ between the conduction and the valence bands. The momenta \mathbf{p} in $\phi_{\mathbf{p}}$ are restricted to the first Brillouin zone. The \mathbf{x} integral is over a unit cell, and the summation is over all reciprocal-lattice vectors \mathbf{G}, \mathbf{G}' . Energy and crystal momentum conservation restrict this summation considerably. Since K and P are determined by the thermal motion of excitons they are negligible compared to k_e and k_h , which are determined by the scale of the energy gap E_g and the reciprocal-lattice vectors. In this limit the condition for conservation of crystal momentum in Eq. (8) becomes,

$$\mathbf{k}_e + \mathbf{k}_h + \mathbf{G} + \mathbf{G}' \approx 0. \quad (10)$$

In the same limit the energy conservation condition,

$$\frac{\hbar^2 k_e^2}{2m_e} + \frac{\hbar^2 k_h^2}{2m_h} = E_g, \quad (11)$$

puts an upper bound on the quantity $|\mathbf{k}_e + \mathbf{k}_h|$. Numerically, $|\mathbf{k}_e + \mathbf{k}_h| a_{\ell} \leq 5.5$, where a_{ℓ} is the lattice constant. Since for the smallest nonzero reciprocal-lattice vector \mathbf{G}_0 , $G_0 a_{\ell} = 6.28$, the conservation laws are satisfied only for

$$\mathbf{G} + \mathbf{G}' = 0. \quad (12)$$

Using the fact that for a relative 1s electron-hole state, $\phi_{-\mathbf{q}} = \phi_{\mathbf{q}}$, the final expression for the sum of the matrix elements for processes A and A' in Fig. 1 is,

$$M_A + M_{A'} = \sum_{\mathbf{q}, \mathbf{G}} V_{\text{eff}}(\mathbf{G} - \mathbf{K}) \phi_{\mathbf{q}} \langle u_{v, \mathbf{q} - \mathbf{K}/2} | u_{c, \mathbf{q} + \mathbf{K}/2} \rangle_{\mathbf{G}} \times \delta_{\mathbf{k}_e + \mathbf{k}_h, \mathbf{K} + \mathbf{P}} (\phi_{\mathbf{k}_h - \mathbf{P}/2} \langle u_{c, \mathbf{k}_e} | u_{c, \mathbf{k}_e + \mathbf{K}} \rangle_{-\mathbf{G}} - \phi_{\mathbf{k}_e - \mathbf{P}/2} \langle u_{v, \mathbf{k}_h} | u_{v, \mathbf{k}_h + \mathbf{P}} \rangle_{-\mathbf{G}}). \quad (13)$$

The first term in parentheses in Eq. (13) corresponds to process A and the second to process A' , which enters with a change of sign because the Coulomb exchange couples to the positively charged hole instead of the electron.

In the second class of diagrams, processes B and B' are equivalent to processes A and A' with either the two electrons or the two holes interchanged. For this reason these processes enter with a minus sign relative to A and A' , and we find

$$\begin{aligned}
M_B + M_{B'} = & - \sum_{\mathbf{q}, \mathbf{G}} \phi_{\mathbf{q}} \delta_{\mathbf{k}_e + \mathbf{k}_h, \mathbf{K} + \mathbf{P}} (\phi_{\mathbf{k}_h - \mathbf{P}/2} V_{\text{eff}}(\mathbf{k}_e + \mathbf{G} - \mathbf{q} - \mathbf{K}/2) \langle u_{v, \mathbf{q} - \mathbf{K}/2} | u_{c, \mathbf{k}_e - \mathbf{K}} \rangle - \mathbf{G} \langle u_{c, \mathbf{k}_e} | u_{c, \mathbf{q} + \mathbf{K}/2} \rangle \mathbf{G} \\
& - \phi_{\mathbf{k}_e - \mathbf{K}/2} V_{\text{eff}}(\mathbf{k}_h + \mathbf{G} - \mathbf{q} - \mathbf{P}/2) \langle u_{v, \mathbf{k}_h - \mathbf{P}} | u_{c, \mathbf{q} - \mathbf{P}/2} \rangle - \mathbf{G} \langle u_{v, \mathbf{k}_h} | u_{v, \mathbf{q} + \mathbf{P}/2} \rangle \mathbf{G}.
\end{aligned} \tag{14}$$

We now consider the effects of the band structure of Cu_2O on the generalized overlap integral, Eq. (9). For $\mathbf{G} = 0$, Eq. (9) is the usual overlap integral between the conduction and the valence bands.¹⁴ We note that for $K = 0$, the wave vector of condensed excitons, the overlap integral for $\mathbf{G} = 0$ vanishes as a consequence of orthogonality of Bloch wave functions between different bands.

The excitons in Cu_2O in the condensation experiments under study are formed from electrons in the lowest conduction band (Γ_6^+) and holes in the highest valence band (Γ_7^+) (the ‘‘yellow series’’). The fact that these two bands have even parity¹⁵ implies that

$$u_{j, \mathbf{k}}(-\mathbf{x}) = u_{j, -\mathbf{k}}(\mathbf{x}). \tag{15}$$

This result is readily seen in the tight-binding approximation for the Bloch wave functions for which

$$\Phi_{j, \mathbf{k}}(\mathbf{x}) = \sum_{\mathbf{R}} \Phi_{a, j}(\mathbf{x} - \mathbf{R}) e^{i\mathbf{k} \cdot \mathbf{R}}, \tag{16}$$

where the summation is over all crystal points and the $\Phi_{a, j}(\mathbf{x})$ are the atomic orbitals which form the band with index j ; for positive parity,

$$\Phi_{j, \mathbf{k}}(-\mathbf{x}) = \Phi_{j, -\mathbf{k}}(\mathbf{x}), \tag{17}$$

from which Eq. (15) follows. Thus, for the $\mathbf{G} = 0$ term in the sum over \mathbf{q} in the matrix elements M_A and $M_{A'}$,

$$\begin{aligned}
& \sum_{\mathbf{q}} \phi_{\mathbf{q}} \langle u_{v, \mathbf{q} - \mathbf{K}/2} | u_{c, \mathbf{q} + \mathbf{K}/2} \rangle_{\mathbf{G} = 0} \\
& = \sum_{\mathbf{q}} \phi_{\mathbf{q}} \langle u_{v, \mathbf{q} + \mathbf{K}/2} | u_{c, \mathbf{q} - \mathbf{K}/2} \rangle_{\mathbf{G} = 0},
\end{aligned} \tag{18}$$

which implies that the sum is an even function of K and is thus proportional to K^2 (since it vanishes for $K = 0$). We use $\mathbf{k} \cdot \mathbf{p}$ perturbation theory¹⁶ to calculate the overlap integral in the above matrix element. For example,

$$|u_{c, \mathbf{q} + \mathbf{K}/2}\rangle \approx |u_{c, \mathbf{q}}\rangle + \frac{\hbar}{m} \sum_{i \neq c} \frac{\langle u_{i, \mathbf{q}} | \mathbf{K}/2 \cdot \mathbf{p} | u_{c, \mathbf{q}} \rangle}{\varepsilon_{c, \mathbf{q}} - \varepsilon_{i, \mathbf{q}}} |u_{i, \mathbf{q}}\rangle, \tag{19}$$

The sum is over all the negative-parity bands of Cu_2O . Of the ten valence and four conduction bands in this material, only the conduction band (c') that is ≈ 449 meV higher than the Γ_6^+ conduction band (c) and the one very deep valence band (v') ≈ 5.6 eV below the Γ_7^+ valence band (v) have odd parity, Fig. 5. The contribution of the odd-parity conduction band is expected to dominate the sum because of the small energy denominator in Eq. (19). Thus

$$\begin{aligned}
& \langle u_{v, \mathbf{q} - \mathbf{K}/2} | u_{c, \mathbf{q} + \mathbf{K}/2} \rangle \\
& \approx \left(\frac{\hbar}{m} \right)^2 \sum_{i \neq c, v} \frac{\langle u_{v, \mathbf{q}} | -\mathbf{K}/2 \cdot \mathbf{p} | u_{i, \mathbf{q}} \rangle \langle u_{i, \mathbf{q}} | \mathbf{K}/2 \cdot \mathbf{p} | u_{c, \mathbf{q}} \rangle}{(\varepsilon_{c, \mathbf{q}} - \varepsilon_{i, \mathbf{q}})(\varepsilon_{i, \mathbf{q}} - \varepsilon_{v, \mathbf{q}})}.
\end{aligned} \tag{20}$$

The $\mathbf{G} = 0$ term (which we denote by ‘‘normal’’) in the sum in Eq. (13) for the matrix elements $M_A + M_{A'}$, in the limit $K, P \ll k_e, k_h$, is equal to

$$\begin{aligned}
(M_A + M_{A'})_{\text{normal}} & = \frac{4\pi e^2}{\Omega \varepsilon_{\infty} K^2} (\phi_{\mathbf{k}_e - \mathbf{K} - \mathbf{P}/2} - \phi_{\mathbf{k}_e - \mathbf{P}/2}) \sum_{\mathbf{q}} \phi_{\mathbf{q}} \langle u_{v, \mathbf{q} - \mathbf{K}/2} | u_{c, \mathbf{q} + \mathbf{K}/2} \rangle \delta_{\mathbf{k}_e + \mathbf{k}_h, \mathbf{K} + \mathbf{P}} \\
& \approx \frac{4\pi e^2}{\Omega \varepsilon_{\infty} K^2} \mathbf{K} \cdot \left(\frac{\partial \phi_{\mathbf{k}}}{\partial \mathbf{k}} \right)_{\mathbf{k}_e} \sum_{\mathbf{q}} \phi_{\mathbf{q}} \langle u_{v, \mathbf{q} - \mathbf{K}/2} | u_{c, \mathbf{q} + \mathbf{K}/2} \rangle \delta_{\mathbf{k}_e + \mathbf{k}_h, \mathbf{K} + \mathbf{P}}.
\end{aligned} \tag{21}$$

As we have shown in Ref. 17 a trial hydrogenic wave function for the 1s-state excitons in Cu_2O with a Bohr radius $a_B \approx 5.3$ Å gives very satisfactory results for the binding energy as well as the total exciton mass. Thus, the assumption that $\Phi_{\text{rel}}(\mathbf{x})$ is approximately the hydrogenic ground-state wave function with an excitonic Bohr radius of 5.3 Å is expected to be quite reliable. An estimate of the above quantity is then,

$$\begin{aligned}
(M_A + M_{A'})_{\text{normal}} & \approx - \frac{2^7 \pi e^2}{\Omega \varepsilon_{\infty}} \frac{(\mathbf{k}_e a_B) \cdot (\mathbf{K} a_B)}{[1 + (k_e a_B)^2]^3} \frac{\hbar^2}{m^2} \\
& \times \sum_{i \neq c, v} \frac{(\mathbf{K} \cdot \mathbf{p}_{v, i})(\mathbf{K} \cdot \mathbf{p}_{i, c})}{K^2 (\varepsilon_{c, 0} - \varepsilon_{i, 0})(\varepsilon_{i, 0} - \varepsilon_{v, 0})} \\
& \times \delta_{\mathbf{k}_e + \mathbf{k}_h, \mathbf{K} + \mathbf{P}},
\end{aligned} \tag{22}$$

where $\mathbf{p}_{i,j}$ is the matrix element of the momentum operator between the Bloch states of the bands i and j at the zone center. The matrix elements $\mathbf{p}_{i,j}$ can be extracted from experiment; if we assume, for example, that they are all of equal magnitude, then Ref. 18 implies that $|\mathbf{p}_{i,j}|/\hbar \approx 0.13 \text{ \AA}^{-1}$.

If K and P are ignored compared to k_e and k_h , in the case that $\mathbf{G}=0$, the right side of Eq. (13) vanishes. The contribution of Umklapp processes to Eq. (13) is,

$$(M_A + M_{A'})_{\text{Umklapp}} \approx \sum_{\mathbf{q}, \mathbf{G} \neq 0} V_{\text{eff}}(\mathbf{G}) \phi_{\mathbf{q}} \phi_{\mathbf{k}_e} \langle u_{v,\mathbf{q}} | u_{c,\mathbf{q}} \rangle_{\mathbf{G}} \\ \times (\langle u_{c,\mathbf{k}_e} | u_{c,\mathbf{k}_e} \rangle_{-\mathbf{G}} \\ - \langle u_{v,\mathbf{k}_h} | u_{v,\mathbf{k}_h} \rangle_{-\mathbf{G}}) \delta_{\mathbf{k}_e + \mathbf{k}_h, \mathbf{K} + \mathbf{P}}, \quad (23)$$

which is nonzero, but very small. In the nearly-free-electron model, for example, with $u_{v,\mathbf{k}}(\mathbf{x}) = 1/\sqrt{\Omega_c}$ and $u_{c,\mathbf{k}}(\mathbf{x}) = e^{i\mathbf{G}_0 \cdot \mathbf{x}}/\sqrt{\Omega_c}$, where Ω_c is the volume of the unit cell and \mathbf{G}_0 one of the six smallest reciprocal-lattice vectors, the right side of Eq. (23) vanishes.

We turn now to the processes B and B' . In the limit $K, P \ll k_e, k_h$ Eq. (14) reduces to

$$M_B + M_{B'} \approx - \sum_{\mathbf{q}, \mathbf{G}} \phi_{\mathbf{q}} \delta_{\mathbf{k}_e + \mathbf{k}_h, \mathbf{K} + \mathbf{P}} (\phi_{\mathbf{k}_h} V_{\text{eff}}(\mathbf{k}_e + \mathbf{G} - \mathbf{q}) \\ \times \langle u_{c,\mathbf{k}_e} | u_{c,\mathbf{q}} \rangle_{\mathbf{G}} \langle u_{v,\mathbf{q}} | u_{c,\mathbf{k}_e} \rangle_{-\mathbf{G}} \\ - \phi_{\mathbf{k}_e} V_{\text{eff}}(\mathbf{k}_h + \mathbf{G} - \mathbf{q}) \\ \times \langle u_{v,\mathbf{k}_h} | u_{c,\mathbf{q}} \rangle_{-\mathbf{G}} \langle u_{v,\mathbf{q}} | u_{v,\mathbf{k}_h} \rangle_{\mathbf{G}}). \quad (24)$$

For $\mathbf{G} \neq 0$, in the same nearly-free-electron approximation, the right side of Eq. (24) vanishes. Since the overlap integrals are less than unity in magnitude, an upper bound of the $\mathbf{G}=0$ term is given by

$$(M_B + M_{B'})_{\text{normal}} \leq 2 \phi_{\mathbf{k}_e} \sum_{\mathbf{q}} \phi_{\mathbf{q}} V_{\text{eff}}(\mathbf{k}_e - \mathbf{q}) \\ \times \langle u_{v,\mathbf{q}} | u_{c,\mathbf{k}_e} \rangle \delta_{\mathbf{k}_e + \mathbf{k}_h, \mathbf{K} + \mathbf{P}}. \quad (25)$$

The overlap integral above is approximately

$$\langle u_{v,\mathbf{q}} | u_{c,\mathbf{k}_e} \rangle \approx \left(\frac{\hbar}{m} \right)^2 \sum_i \frac{(\mathbf{q} - \mathbf{k}_e) \cdot \mathbf{p}_{c,i} (\mathbf{q} - \mathbf{k}_e) \cdot \mathbf{p}_{i,v}}{(\varepsilon_{c,0} - \varepsilon_{i,0})(\varepsilon_{i,0} - \varepsilon_{v,0})}, \quad (26)$$

where q ranges approximately between $k_e - 1/a_l$ and $k_e + 1/a_l$. Then,

$$(M_B + M_{B'})_{\text{normal}} \leq 41 \frac{e^2}{\Omega \varepsilon_{\infty}} \frac{1}{[1 + (k_e a_B)^2]^2} \left(\frac{\hbar}{m} \right)^2 \\ \times \sum_i \frac{|\mathbf{p}_{c,i}| |\mathbf{p}_{i,v}|}{(\varepsilon_{c,0} - \varepsilon_{i,0})(\varepsilon_{i,0} - \varepsilon_{v,0})} \delta_{\mathbf{k}_e + \mathbf{k}_h, \mathbf{K} + \mathbf{P}}, \quad (27)$$

where the numerical factor is the result of a dimensionless integral times constants. We show below using Eq. (27) that processes B and B' contribute negligibly to the Auger decay rate. Only A and A' contribute significantly to the direct

Auger mechanism; these processes do not allow condensed excitons to Auger recombine, since $M_A + M_{A'}$ vanishes for $K=0$ [Eq. (22)].

We next proceed to calculate the decay rate $\Gamma_{\mathbf{K},\mathbf{P}}$ for the direct process in which two excitons of momentum \mathbf{K} and \mathbf{P} collide. From the golden rule

$$\Gamma_{\mathbf{K},\mathbf{P}} = \frac{2\pi}{\hbar} \sum_{\mathbf{k}_e, \mathbf{k}_h} |M|^2 (1 - n_{c,\mathbf{k}_e})(1 - n_{v,\mathbf{k}_h}) \\ \times \delta(E_{\mathbf{K}} + E_{\mathbf{P}} - \varepsilon_{c,\mathbf{k}_e} - \varepsilon_{v,\mathbf{k}_h}), \quad (28)$$

where M is the matrix element for the process. The exciton energies are

$$E_{\mathbf{Q}} = E_g - E_b + \frac{\hbar^2 Q^2}{2M_{\text{exc}}}, \quad (29)$$

where M_{exc} is the exciton mass, E_b is the binding energy, ≈ 141 meV including the exchange energy $\Delta E \approx 12$ meV which is nonzero for the ortho excitons only (see Sec. III). We may neglect E_b and ΔE compared to the energy gap E_g . The electron and the hole energies are

$$\varepsilon_{c,\mathbf{k}_e} = E_g + \frac{\hbar^2 k_e^2}{2m_e}, \quad \varepsilon_{v,\mathbf{k}_h} = \frac{\hbar^2 k_h^2}{2m_h}, \quad (30)$$

and the n_{j,\mathbf{k}_i} 's are the electron and hole occupation numbers in the final ionized states. Since these final states have very high energy, we may neglect the n_{j,\mathbf{k}_i} in Eq. (28), as well as the inverse process.

The decay rate per unit volume for the direct Auger process, $\Gamma_{A,d}/\Omega$, is given by

$$\frac{1}{\Omega} \Gamma_{A,d} = - \frac{1}{\Omega} \left(\frac{\partial N}{\partial t} \right)_{A,d} = \frac{1}{\Omega} \sum_{\mathbf{K},\mathbf{P}} f_{\mathbf{K}} f_{\mathbf{P}} \Gamma_{\mathbf{K},\mathbf{P}} \equiv \frac{n}{\tau_{A,d}}, \quad (31)$$

where $f_{\mathbf{K}}$ is the distribution function of excitons, n is the density of excitons, and $\tau_{A,d}$ is the scattering time for the direct Auger process.

Using Eq. (22) we estimate the contribution to the decay rate due to the (dominant) processes A and A'

$$\tau_{A,d}^{-1} \approx 0.77 \times 2^{17} \pi^2 \frac{\mu e^4}{2\hbar^3 \varepsilon_{\infty}^2} \frac{(k_g a_B)^3}{[(k_g a_B)^2 + 1]^6} \frac{M_{\text{exc}} a_B^2}{\hbar^2} \left(\frac{\hbar}{m a_B} \right)^4 \\ \times \sum_i \left(\frac{|\mathbf{p}_{c,i}| |\mathbf{p}_{i,v}|}{(\varepsilon_{c,0} - \varepsilon_{i,0})(\varepsilon_{i,0} - \varepsilon_{v,0})} \right)^2 k_B T n_{\text{exc}} a_B^3, \quad (32)$$

where $E_g \equiv \hbar^2 k_g^2 / 2\mu$, μ is the reduced mass for the electron and the hole, n_{exc} is the density of noncondensed (excited) excitons, and T is the temperature of the exciton gas. We note that $\tau_{A,d}$ is inversely proportional to the density of noncondensed excitons. For the proportionality constant for excitons in Cu_2O ,

$$\tau_{A,d}^{-1} \approx 4 \times 10^{-3} n_{\text{exc}} T \text{ ns}^{-1}, \quad (33)$$

with T measured in Kelvin and n_{exc} measured in units of 10^{18} cm^{-3} . As we will see this decay rate is small compared to the rate for the phonon-assisted process, but it can contribute to para-exciton para-exciton Auger collisions (which

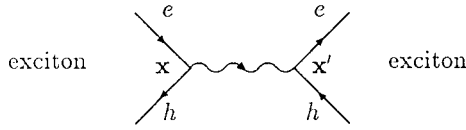


FIG. 3. Virtual annihilation diagram of an exciton, possible only for pure spin-singlet excitons.

are, as we will see, forbidden in the zero-stress case) in highly stressed crystals. We explain this effect in the next section.

Finally Eq. (27) gives an upper bound for $\tau_{A,d;B+B'}^{-1}$, i.e., the contribution of processes B and B' to $\tau_{A,d}^{-1}$,

$$\tau_{A,d;B+B'}^{-1} \leq \frac{2 \times 41^2}{\pi} \frac{\mu e^4}{2 \hbar^3 \epsilon_\infty^2} \frac{(k_g a_B)}{[1 + (k_g a_B)^2]^4} \left(\frac{\hbar}{m a_B} \right)^4 \times \sum_i \left(\frac{|\mathbf{p}_{c,i}| |\mathbf{p}_{i,v}|}{(\epsilon_{c,0} - \epsilon_{i,0})(\epsilon_{i,0} - \epsilon_{v,0})} \right)^2 n a_B^3. \quad (34)$$

For the parameters of excitons in Cu_2O , Eq. (34) gives $\tau_{A,d;B+B'}^{-1} \leq 3 \times 10^{-3} n \text{ ns}^{-1}$, with n measured in units of 10^{18} cm^{-3} , which is negligible compared with the contribution of the processes A and A' as well as the most important processes of the phonon-assisted Auger mechanism.

III. SPIN STATISTICS — BAND STRUCTURE AND OPTICAL PROPERTIES OF Cu_2O

In this section we review the band structure underlying the properties of excitons in Cu_2O and their direct Auger recombination process. These properties influence the direct as well as the phonon-assisted mechanisms. We discuss the effects of the band structure on the phonon-assisted Auger process in Sec. IV.

The direct radiative recombination of both ortho and para excitons is dipole forbidden because the conduction and valence bands have the same parity.^{15,19} The quadrupole recombination of ortho excitons is allowed and has been observed experimentally.²⁰ In contrast, the direct radiative recombination of para excitons is highly forbidden,²¹ but becomes allowed if uniaxial stress is applied.²² Both species can recombine via phonon-assisted processes.

The exchange interaction, shown in Fig. 3, where an exciton virtually annihilates and reforms, is responsible for the ortho-para energy splitting at the zone center of Cu_2O . Although for pure spin states this interaction is nonzero for the singlet, shifting the energy of the singlet state higher than the triplet, experimentally the ortho excitons lie higher than the para excitons by 12 meV.⁵ The absorption spectrum of Cu_2O (Refs. 19 and 23) shows discrete lines below the continuum which correspond to excitonic absorption, but the $n=1$ line is very weak, in contrast with the $n=2,3, \dots$ lines. All these observations can be understood in terms of the band structure of Cu_2O .¹⁵ The conduction band is formed by Cu $4s$ orbitals and the valence band by Cu $3d$ orbitals. The fivefold degenerate (without spin) Cu $3d$ orbitals split under the crystal field into a higher threefold Γ_{25}^+ and

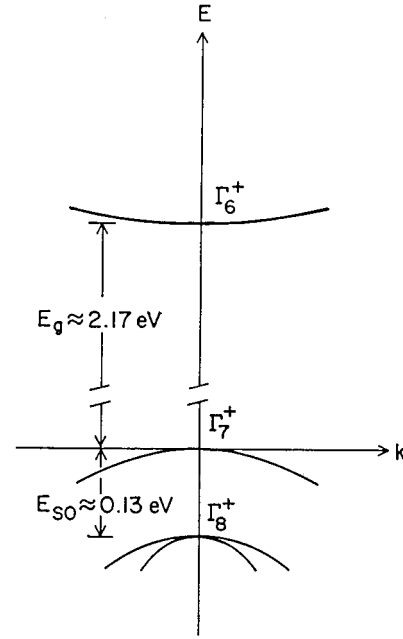


FIG. 4. Schematic band structure of Cu_2O showing the conduction Γ_6^+ band and the Γ_7^+, Γ_8^+ valence bands (split by the spin-orbit splitting) which form the yellow and green exciton series, respectively.

a lower twofold degenerate band Γ_{12}^+ . Finally, Γ_{25}^+ splits further because of the spin-orbit interaction into two bands, a higher Γ_7^+ nondegenerate band and a lower twofold degenerate Γ_8^+ band (Fig. 4). The Γ_7^+ and Γ_8^+ mix with the Γ_6^+ conduction band to form the yellow- and green-exciton series, respectively.

From now on we restrict our discussion to the yellow-exciton series. The weakness of the $n=1$ line in the absorption spectrum is due to the Γ_6^+ and Γ_7^+ bands having the same parity, making the transition to this line only quadrupole-allowed. In contrast to the $n=1$ line, the $n=2,3, \dots$ lines are dipole active, provided that the created excitons are in p states. The total angular momentum functions for the exciton triplet states are

$$|J=1, J_z=1\rangle = |\uparrow_e, \uparrow_H\rangle, \quad (35)$$

$$|J=1, J_z=0\rangle = \frac{1}{\sqrt{2}} (|\uparrow_e, \downarrow_H\rangle - |\downarrow_e, \uparrow_H\rangle), \quad (36)$$

$$|J=1, J_z=-1\rangle = |\downarrow_e, \downarrow_H\rangle, \quad (37)$$

and for the singlet states,

$$|J=0, J_z=0\rangle = \frac{1}{\sqrt{2}} (|\uparrow_e, \downarrow_H\rangle + |\downarrow_e, \uparrow_H\rangle). \quad (38)$$

The indices e, H refer to the electron and the hole, respectively; while the electron states are pure spin states, the hole states are *total* angular momentum states,

$$|\uparrow_H\rangle = -\frac{1}{\sqrt{3}}[(X+iY)|\downarrow_h\rangle + Z|\uparrow_h\rangle] \quad (39)$$

and

$$|\downarrow_H\rangle = -\frac{1}{\sqrt{3}}[(X-iY)|\uparrow_h\rangle - Z|\downarrow_h\rangle], \quad (40)$$

where the states with lower case h are pure spin states. The spatial functions X, Y, Z transform as $yz, xz,$ and $xy,$ respectively.

Using these angular momentum functions we explain now the experimental observations mentioned above, turning to the direct Auger decay process at the end of the section. In the radiative recombination of an exciton the electron goes from the conduction to the valence band with emission of a photon. If we assume that there is no spin-flip (a higher-order effect), the above angular momentum functions imply that the matrix element for the direct radiative recombination rate for the ortho excitons is proportional to $\sqrt{2/3}$ times the result of the spatial part of the calculation, but that it vanishes for the para excitons. Similarly, para excitons are not allowed to recombine directly and the exchange interaction vanishes for the singlet. For the triplet state the exchange interaction is nonzero and raises the ortho-exciton energy with respect to the para-exciton energy; the energy splitting ΔE at the zone center ($K=0$) is given by⁵

$$\Delta E = \frac{2}{3} \int \Psi_{\mathbf{K}=0}(\mathbf{x}, \mathbf{x}) \frac{e^2}{\epsilon_\infty |\mathbf{x} - \mathbf{x}'|} \Psi_{\mathbf{K}=0}^*(\mathbf{x}', \mathbf{x}') d\mathbf{x} d\mathbf{x}', \quad (41)$$

where the factor of $2/3$ again comes from the angular momentum wave functions. Using Eq. (3) for the exciton wave function we find that

$$\Delta E = \frac{2}{3} \sum_{\mathbf{q}, \mathbf{p}, \mathbf{G} \neq 0} \frac{4\pi e^2}{\Omega |\mathbf{G}|^2 \epsilon_\infty} \phi_{\mathbf{q}} \langle u_{v, \mathbf{q}} | u_{c, \mathbf{q}} \rangle_{\mathbf{G}} \phi_{\mathbf{p}}^* \langle u_{v, \mathbf{p}} | u_{c, \mathbf{p}} \rangle_{\mathbf{G}}^*. \quad (42)$$

The sum is dominated by the terms with smallest \mathbf{G} 's (six in number because of the cubic symmetry of the crystal), which we denote by G_0 ; then

$$\begin{aligned} \Delta E &\approx \frac{12}{3} \frac{4\pi e^2}{\Omega \epsilon_\infty} \Omega |\phi_{\text{rel}}(0)|^2 \frac{a_c^2}{4\pi^2} |\langle u_{v, 0} | u_{c, 0} \rangle_{\mathbf{G}_0}|^2 \\ &= \frac{e^2}{a_B \epsilon_0} \frac{4}{\pi^2} \frac{\epsilon_0}{\epsilon_\infty} \left(\frac{a_c}{a_B} \right)^2 |\langle u_{v, 0} | u_{c, 0} \rangle_{\mathbf{G}_0}|^2. \end{aligned} \quad (43)$$

Since experimentally $\Delta E \approx 12 \text{ meV}$,²⁴ we have $|\langle u_{v, 0} | u_{c, 0} \rangle_{\mathbf{G}_0}| \approx 0.45$.

In Auger decay, processes B and B' are not affected by the angular momentum of the electron and the hole. The forbiddenness of the direct radiative recombination of the para excitons due to the spin conservation implies that the recombination vertices which appear in processes A and A' of Fig. 1 are nonzero *only* for an ortho exciton decaying and ionizing with *either* an ortho exciton or a para exciton.

Uniaxial stress mixes the Γ_7^+ and Γ_8^+ valence bands with the results that the para-exciton energy increases for small values of the applied stress but decreases for higher values, and the direct radiative recombination increases quadratically with increasing stress.²² In the Auger process this mixing implies that the recombination vertex of stressed para excitons becomes allowed. Para excitons in highly stressed crystals are therefore able to Auger recombine (processes A and A'), ionizing either an ortho exciton or a para exciton, just like the ortho excitons in the unstressed case. We discuss this effect further in Sec. VI.

IV. PHONON-ASSISTED AUGER PROCESS

The phonon-assisted Auger mechanism with the participation of a longitudinal, odd-parity optical phonon is in fact the dominant Auger process. Although this process requires a phonon and its rate is therefore reduced by factors of the exciton-phonon interaction, the dipole matrix element between the intermediate state and the conduction or the valence band does not vanish, in contrast to the case of the direct Auger mechanism. Since the matrix element for normal processes ($\mathbf{G}=0$) does not vanish for $K=0$, the contribution of Umklapp processes should be relatively small, and we neglect them. In this case the angular momentum of the colliding excitons does not put any restriction on Auger collisions. Following the same procedure as before, we calculate all Feynman diagrams (Fig. 2). We assume for simplicity that the lattice temperature is very low, and only spontaneous phonon emission is possible.

For the processes C, C' and D, D' of Fig. 2 with two excitons of momentum \mathbf{K} and \mathbf{P} colliding, giving an electron of momentum \mathbf{k}_e , a hole of momentum \mathbf{k}_h and a longitudinal optical (LO) phonon of momentum \mathbf{Q} and energy $\hbar\omega_{\mathbf{Q}}$, denoted by the dashed line, the matrix element is

$$\begin{aligned} M_C + M_{C'} + M_D + M_{D'} &= V_{\text{eff}}(\mathbf{K} - \mathbf{Q}) (\phi_{\mathbf{k}_h - \mathbf{P}/2} - \phi_{\mathbf{k}_e - \mathbf{P}/2}) \sum_{\mathbf{q}, n} \phi_{\mathbf{q}} \left(\frac{\langle u_{v, \mathbf{q} - \mathbf{K}/2} | u_{n, \mathbf{q} + \mathbf{K}/2 - \mathbf{Q}} \rangle \langle u_{n, \mathbf{q} + \mathbf{K}/2 - \mathbf{Q}} | H_{\text{LO}} | u_{c, \mathbf{q} + \mathbf{K}/2} \rangle}{\epsilon_{c, \mathbf{q} + \mathbf{K}/2} - \epsilon_{n, \mathbf{q} + \mathbf{K}/2 - \mathbf{Q}} - \hbar\omega_{\mathbf{Q}}} \right. \\ &\quad \left. + \frac{\langle u_{v, \mathbf{q} - \mathbf{K}/2} | H_{\text{LO}} | u_{n, \mathbf{q} - \mathbf{K}/2 + \mathbf{Q}} \rangle \langle u_{n, \mathbf{q} - \mathbf{K}/2 + \mathbf{Q}} | u_{c, \mathbf{q} + \mathbf{K}/2} \rangle}{\epsilon_{v, \mathbf{q} - \mathbf{K}/2} - \epsilon_{n, \mathbf{q} - \mathbf{K}/2 + \mathbf{Q}} + \hbar\omega_{\mathbf{Q}}} \right) \delta_{\mathbf{k}_e + \mathbf{k}_h + \mathbf{Q}, \mathbf{K} + \mathbf{P}}, \end{aligned} \quad (44)$$

where H_{LO} is the carrier (i.e., electron or hole), LO-phonon interaction. The first term in the sum refers to processes C and C' , and the second to processes D and D' . The sum over n includes the two odd-parity bands of Cu_2O . We again use $\mathbf{k} \cdot \mathbf{p}$ perturbation theory to calculate the overlap integrals in the above matrix element. For example,

$$\langle u_{v,q-\mathbf{K}/2} | u_{n,q+\mathbf{K}/2} \rangle \approx \frac{\hbar}{m} \frac{\langle u_{v,q-\mathbf{K}/2} | (\mathbf{Q}-\mathbf{K}) \cdot \mathbf{p} | u_{n,q-\mathbf{K}/2} \rangle}{\varepsilon_{n,q-\mathbf{K}/2} - \varepsilon_{v,q-\mathbf{K}/2}}. \quad (45)$$

The two terms in the sum of Eq. (44) are closely related to the matrix elements for radiative phonon-assisted exciton recombination. We show the radiative recombination processes of an exciton in Fig. 2, diagrams F and F' , where an exciton recombines emitting a phonon of momentum \mathbf{Q} and a photon of momentum \mathbf{k}_γ . The similarity of the upper part of diagrams C , C' , D , and D' with F and F' , enables us to extract information about the phonon-assisted Auger mechanism. Experimentally, the primary luminescence mechanism of ortho excitons in Cu_2O is via phonon-assisted recombination involving the Γ_{12}^- optical phonon. Other phonon-assisted recombination processes of the ortho excitons are at least 30 times weaker. For the para excitons the only allowed optical phonon recombination mechanism is via a Γ_{25}^- phonon, and the integrated intensity is about 500 times weaker than the Γ_{12}^- ortho-exciton phonon-assisted mechanism. This difference is due to the band structure of the material and the symmetry of the bands that are involved in the transition. Group theory allows both odd-parity bands to assist the ortho-exciton radiative recombination, so for the orthoexcitons both processes F and F' are allowed. In para-exciton recombination, in contrast, only the deep valence band can be the intermediate state (diagram F'), as illustrated in Fig. 5.²⁴ This analysis is valid only for nonstressed crystals; if stress is applied the mixing between the Γ_7^+ and the Γ_8^+ valence bands, dependent on the orientation of the applied stress, is expected to affect the phonon-assisted radiative recombination processes.

In the Auger problem this symmetry argument implies that for ortho-exciton recombination, the rate due to processes C and C' is much larger than the rate due to D and D' . For para excitons, processes C and C' are forbidden and D and D' contribute negligibly to the decay rate. To estimate the ratio of the magnitudes of the matrix elements for the faster ortho-exciton ($M_C + M_{C'}$) and the para-exciton ($M_D + M_{D'}$) Auger phonon-assisted mechanisms due to this effect we note that the only difference in this case as compared to the radiative recombination comes from the energy denominator in Eq. (45). An estimate of this ratio is

$$\left| \frac{M_C + M_{C'}}{M_D + M_{D'}} \right| \approx \sqrt{\frac{\Gamma_{o,\text{rad}}}{\Gamma_{p,\text{rad}}}} \frac{\varepsilon_{c',0} - \varepsilon_{v,0}}{\varepsilon_{c,0} - \varepsilon_{v',0}} \approx \sqrt{500} \frac{\varepsilon_{c',0} - \varepsilon_{v,0}}{\varepsilon_{c,0} - \varepsilon_{v',0}}, \quad (46)$$

where $\Gamma_{o,\text{rad}}$ is the total decay rate of ortho excitons due to the Γ_{12}^- phonon and $\Gamma_{p,\text{rad}}$ is the total decay rate of para excitons due to the Γ_{25}^- phonon. As can be seen from the energy differences in the denominator of Eq. (46) using the energy levels of Cu_2O , $|(M_C + M_{C'})/(M_D + M_{D'})| \approx 3.0 \times \sqrt{500}$. The only assumption we have made in writing

Eq. (46) is the reasonable one that the oscillator strengths between the bands c' , v , and c, v' are comparable. Thus, the relative decay rate due to processes C, C' as compared with the decay rate of D, D' is $\approx 5 \times 10^3$. Since, as we show below, all other diagrams (of the form of E in Fig. 2) for the phonon-assisted Auger mechanism can be neglected, we conclude that para excitons have a negligible phonon-assisted Auger decay rate (in para-para collisions), compared with the ortho excitons, in agreement with the observed long para-exciton lifetime when no ortho excitons are present. Since the Γ_{12}^- optical phonon dominates the phonon-assisted Auger decay process of ortho excitons, we neglect the contribution of all other phonons.

Expanding the overlap integral $\langle u_{v,q-\mathbf{K}/2} | u_{c',q+\mathbf{K}/2} \rangle$ in powers of $\mathbf{K}-\mathbf{Q}$, using $\mathbf{k} \cdot \mathbf{p}$ perturbation theory, we see that the matrix element for processes C and C' goes as

$$M_C + M_{C'} \sim \frac{1}{|\mathbf{K}-\mathbf{Q}|^2} (\phi_{\mathbf{k}_e - \mathbf{P}/2 - \mathbf{K} + \mathbf{Q}} - \phi_{\mathbf{k}_e - \mathbf{P}/2}) \times (\mathbf{K}-\mathbf{Q}) \cdot \mathbf{p}_{v,c'}, \quad (47)$$

so the matrix element $M_C + M_{C'}$ can be treated as constant. We estimate it using Eqs. (44) and (45) as

$$M_C + M_{C'} \approx \frac{1}{\Omega} (\mathbf{K}-\mathbf{Q}) \cdot \left(\frac{\partial \phi_{\mathbf{p}}}{\partial \mathbf{p}} \right)_{\mathbf{k}_e} \frac{4\pi e^2}{\varepsilon_{\infty} |\mathbf{K}-\mathbf{Q}|^2} \times \left(\sum_{\mathbf{q}} \phi_{\mathbf{q}} \right) \frac{\hbar}{m} \frac{\mathbf{p}_{v,c'} \cdot (\mathbf{K}-\mathbf{Q})}{(\varepsilon_{c',0} - \varepsilon_{v,0})} \times \frac{\langle u_{c',0} | H_{\Gamma_{12}^-} | u_{c,0} \rangle}{(\varepsilon_{c,0} - \varepsilon_{c',0})} \delta_{\mathbf{k}_e + \mathbf{k}_h + \mathbf{Q}, \mathbf{K} + \mathbf{P}}. \quad (48)$$

The matrix element $\langle u_{c',0} | H_{\Gamma_{12}^-} | u_{c,0} \rangle$ equals $D_{\Gamma_{12}^-} [\hbar / (2\rho\Omega\omega_{\Gamma_{12}^-})]^{1/2}$ in magnitude, where $\omega_{\Gamma_{12}^-}$ is the zone-center frequency of the specific phonon, ≈ 13.8 meV, ρ is the mass density of the material, and $D_{\Gamma_{12}^-}$ is the deformation potential involving the Γ_{12}^- optical phonon-mediated interband transition between the Γ_6^+ and the c' band. Therefore, Eq. (48) can be written as

$$M_C + M_{C'} \approx 128\pi \frac{e^2 a_B \hbar}{\varepsilon_{\infty} \Omega m} \frac{|\mathbf{p}_{v,c'}|}{(\varepsilon_{c',0} - \varepsilon_{v,0})} \frac{k_e a_B}{[1 + (k_e a_B)^2]^3} \times \frac{D_{\Gamma_{12}^-}}{(\varepsilon_{c,0} - \varepsilon_{c',0})} \left(\frac{\hbar}{2\rho\Omega\omega_{\Gamma_{12}^-}} \right)^{1/2} \delta_{\mathbf{k}_e + \mathbf{k}_h + \mathbf{Q}, \mathbf{K} + \mathbf{P}}. \quad (49)$$

The deformation potential $D_{\Gamma_{12}^-}$ has not been measured directly, but we can extract an estimate from Ref. 21. We use the measured para-exciton lifetime of 13 μs at a temperature of 10 K and the relative integrated intensities of the Γ_{12}^- ortho-exciton phonon-assisted mechanism with respect to the Γ_{25}^- para-exciton phonon-assisted mechanism (approximately 500, as mentioned earlier), to fit the decay rate of the ortho excitons due to the phonon-assisted recombination, 26 ns at the same temperature of 10 K. This analysis implies that $D_{\Gamma_{12}^-} \approx 2.5$ eV/Å.

For the processes of the form of E shown in Fig. 2, which correspond to the diagrams B and B' (direct Auger process) with additional emission of a Γ_{12}^- phonon, we have

$$M_E = \sum_{\mathbf{q}} \phi_{\mathbf{q}} \phi_{\mathbf{k}_h - \mathbf{P}/2} V_{\text{eff}}(\mathbf{k}_e - \mathbf{q} - \mathbf{K}/2) \times \frac{\langle u_{v, \mathbf{q} - \mathbf{K}/2} | u_{c', \mathbf{k}_e - \mathbf{K}} \rangle \langle u_{c', \mathbf{k}_e - \mathbf{K}} | H_{\Gamma_{12}^-} | u_{c, \mathbf{P} - \mathbf{k}_h} \rangle}{\varepsilon_{c, \mathbf{k}_h - \mathbf{P}} - \varepsilon_{c', \mathbf{k}_e - \mathbf{K}} - \hbar \omega_{\mathbf{Q}}} \times \delta_{\mathbf{k}_e + \mathbf{k}_h + \mathbf{Q}, \mathbf{K} + \mathbf{P}}. \quad (50)$$

Since the overlap integral is less than unity, an upper bound on M_E is

$$M_E \leq \left| \phi_{\mathbf{k}_h} \frac{\langle u_{c', 0} | H_{\Gamma_{12}^-} | u_{c, 0} \rangle}{\varepsilon_{c, 0} - \varepsilon_{c', 0}} \sum_{\mathbf{q}} \phi_{\mathbf{q}} V_{\text{eff}}(\mathbf{k}_e - \mathbf{q}) \times \delta_{\mathbf{k}_e + \mathbf{k}_h + \mathbf{Q}, \mathbf{K} + \mathbf{P}} \right|. \quad (51)$$

The sum over \mathbf{q} in Eq. (51), the convolution of the wave function of the relative electron-hole motion $\phi_{\text{rel}}(x)$ times the Coulomb interaction $V_{\text{eff}}(x)$, can be calculated analytically, yielding

$$M_E \leq \frac{1}{\Omega^{1/2}} \phi_{\mathbf{k}_h} \frac{D_{\Gamma_{12}^-}}{(\varepsilon_{c, 0} - \varepsilon_{c', 0})} \left(\frac{\hbar}{2\rho\Omega\omega_{\Gamma_{12}^-}} \right)^{1/2} \times \frac{4(\pi a_B)^{1/2} e^2}{\varepsilon_{\infty} [1 + (k_e a_B)^2]} \delta_{\mathbf{k}_e + \mathbf{k}_h + \mathbf{Q}, \mathbf{K} + \mathbf{P}}. \quad (52)$$

Let us proceed to the calculation of the decay rate. If M_{ph} is the matrix element for the phonon-assisted process, the decay rate of two colliding excitons with momenta \mathbf{K} and \mathbf{P} giving an electron of momentum \mathbf{k}_e , a hole of momentum \mathbf{k}_h with simultaneous emission of an optical phonon of momentum \mathbf{Q} , is

$$\Gamma_{\mathbf{K}, \mathbf{P}} = \frac{2\pi}{\hbar} \sum_{\mathbf{k}_e, \mathbf{k}_h, \mathbf{Q}} |M_{\text{ph}}|^2 (1 - n_{c, \mathbf{k}_e}) (1 - n_{v, \mathbf{k}_h}) \times \delta(E_{\mathbf{K}} + E_{\mathbf{P}} - \hbar \omega_{\mathbf{Q}} - \varepsilon_{c, \mathbf{k}_e} - \varepsilon_{v, \mathbf{k}_h}). \quad (53)$$

We neglect the inverse process at very low lattice temperature, where no phonons are present.

The contribution of the (dominant) processes C and C' to the Auger phonon-assisted decay rate, defined in Eq. (31), is, using Eq. (49),

$$\tau_{A, \text{ph}}^{-1} \approx \frac{2^{16} \times 10^{-2}}{\pi} \frac{\mu e^4}{2\hbar^3 \varepsilon_{\infty}^2} \frac{\hbar^4}{m \rho a_B^7} n a_B^3 \frac{|\mathbf{p}_{c', v}|^2}{m} \times \frac{(D_{\Gamma_{12}^-} a_B)^2}{(\varepsilon_{c, 0} - \varepsilon_{c', 0})^2 (\varepsilon_{c', 0} - \varepsilon_{v, 0})^2 \hbar \omega_{\Gamma_{12}^-}}. \quad (54)$$

In the approximation of Eq. (47), where the matrix element is constant, $\tau_{A, \text{ph}}^{-1}$ is temperature independent at low lattice temperature and the corresponding inverse scattering time is

proportional to the density of the total number of excitons, $\tau_{A, \text{ph}}^{-1} \sim n$. If we measure the density in units of 10^{18} cm^{-3} , Eq. (54) gives the decay rate

$$\tau_{A, \text{ph}}^{-1} \approx 0.8n \text{ ns}^{-1}, \quad (55)$$

which is on the order of magnitude of the observed decay rate, but not numerically accurate.

For process E , the approximate expression on the right side of Eq. (52) for the matrix element yields a lower bound on the contribution $\tau_{A, \text{ph}, E}$ to the Auger phonon-assisted scattering time,

$$\tau_{A, \text{ph}, E}^{-1} \leq \frac{2^{10} \times 10^{-4}}{\pi} \frac{\mu e^4}{2\hbar^3 \varepsilon_{\infty}^2} \frac{\hbar^2}{\rho a_B^5} n a_B^3 \frac{(D_{\Gamma_{12}^-} a_B)^2}{(\varepsilon_{c, 0} - \varepsilon_{c', 0})^2 \hbar \omega_{\Gamma_{12}^-}}. \quad (56)$$

Numerically $\tau_{A, \text{ph}, E}^{-1} \leq 8 \times 10^{-3} n \text{ ns}^{-1}$, with n measured in units of 10^{18} cm^{-3} , which is comparable to the decay rate of the para excitons, i.e., the smallest decay rate of our problem. Processes of the form of E are in fact much slower than this rate, since we have assumed in Eq. (56) that the overlap integral is unity. Furthermore, the process E' , of the form of E with the Coulomb exchange coupling instead of the positively charged hole, enters with a change of sign, partially cancelling E .

V. EFFECTS OF IDENTITY ON THE AUGER DECAY RATE

We turn now to the problem of the identity between the electrons and holes of the two excitons. The total wave function of two excitons of momenta \mathbf{K} and \mathbf{P} with angular momentum functions χ_{α} and χ_{β} , respectively, is

$$\Psi_{i, \text{tot}} = \frac{1}{2} [\Psi_{\mathbf{K}}(1, 2) \chi_{\alpha}(1, 2) \Psi_{\mathbf{P}}(1', 2') \chi_{\beta}(1', 2') - \Psi_{\mathbf{K}}(1', 2) \chi_{\alpha}(1', 2) \Psi_{\mathbf{P}}(1, 2') \chi_{\beta}(1, 2') - \Psi_{\mathbf{K}}(1, 2') \chi_{\alpha}(1, 2') \Psi_{\mathbf{P}}(1', 2) \chi_{\beta}(1', 2) + \Psi_{\mathbf{K}}(1', 2') \chi_{\alpha}(1', 2') \Psi_{\mathbf{P}}(1, 2) \chi_{\beta}(1, 2)], \quad (57)$$

where the variables 1, 1', 3 refer to electrons and 2, 2', 4 to holes. The wave function of the final state is

$$\Psi_{f, \text{tot}} = \Psi_{\mathbf{k}_e, \mathbf{k}_h}(3, 4) \chi_{\gamma}(3, 4). \quad (58)$$

The calculation we have presented has been done without effects of identity taken into account. Thus, if the initial state in the matrix elements M_A , $M_{A'}$, M_C , and $M_{C'}$ is the first term of Eq. (57), the second term of Eq. (57) gives the initial state in the matrix elements M_B , $M_{B'}$, M_D , and $M_{D'}$; the last two give exchange terms. Since the phonon-assisted processes C and C' dominate the Auger collisions, we examine here the effect of identity of the electrons and the holes on the corresponding matrix elements M_C and $M_{C'}$.

The Coulomb interaction does not produce any spin flips, so the angular momentum functions χ_i factor out in all the matrix elements, independent of the spatial part of the calculation. For ortho-para and for ortho-ortho collisions with different J_z , only the first or the last term of Eq. (57) contributes to the matrix element, because of the orthogonality of the angular momentum wave functions. The actual matrix

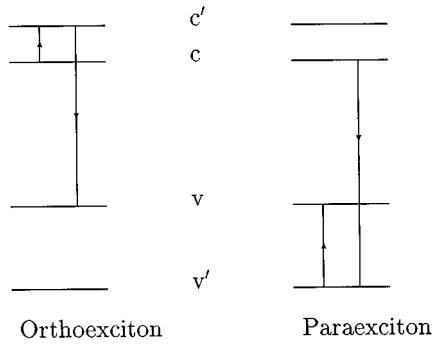


FIG. 5. Phonon-assisted radiative recombination processes. The ortho excitons are allowed to participate in both, but for the para excitons only the one on the right side is allowed. The bands c, v are the Γ_6^+ and the Γ_7^+ bands which form the yellow excitons and are separated by 2.17 eV. The bands c' and v' are the only odd-parity bands in Cu_2O . The energy difference between c' and c is ≈ 449 meV and between v and v' is ≈ 5.6 eV. The proximity of band c' to band c makes both the radiative recombination (Ref. 24) and the phonon-assisted Auger decay processes much faster for ortho excitons than para excitons.

element, therefore, for the case that the effect of identity has been taken into account is $1/2$ (from the normalization constant) times the result of our calculation from the previous section. For ortho-ortho collisions with the same J_z , both the first as well as the last term in Eq. (57) contribute to the matrix element and therefore the numerical factor which multiplies the matrix element in this case is $1/2 + 1/2 = 1$.

In a gas of ortho excitons with random J_z , there are nine possible combinations, with respect to their angular momentum, that two ortho excitons collide. Statistically $3/9$ of the collision events are between ortho excitons with the same J_z , and $6/9$ between ortho excitons with different J_z . Consequently, if C_A [≈ 0.8 from Eq. (55)] is the proportionality factor in our calculation without taking into account the effect of identity, the effect of identity on the decay rate is to multiply the original rate by a factor $(3/9)1 + (6/9)(1/2)^2 = 1/2$ for ortho-ortho collisions and $(1/2)^2$ for ortho-para collisions. Thus for the dominant phonon-assisted Auger process

$$-\frac{1}{N_o} \left(\frac{\partial N_o}{\partial t} \right)_{A, \text{ph}}^o \equiv \frac{1}{\tau_{A, \text{ph}}^o} = \frac{C_A}{2} \left(n_o + \frac{1}{2} n_p \right), \quad (59)$$

$$-\frac{1}{N_p} \left(\frac{\partial N_p}{\partial t} \right)_{A, \text{ph}}^p \equiv \frac{1}{\tau_{A, \text{ph}}^p} = \frac{C_A}{4} n_o, \quad (60)$$

where N_o and N_p are the numbers of ortho and para excitons, respectively. To determine the *net* loss of ortho and para excitons due to the Auger process, we take into account the fact that the Auger-ionized excitons reform in random angular momentum states, and find

$$-\frac{1}{N_o} \left(\frac{\partial N_o}{\partial t} \right)_{A, \text{net}}^o = \frac{C_A}{16} (5n_o + n_p), \quad (61)$$

$$-\frac{1}{N_p} \left(\frac{\partial N_p}{\partial t} \right)_{A, \text{net}}^p = \frac{C_A}{16} n_o \left(3 - \frac{n_o}{n_p} \right). \quad (62)$$

VI. EXPERIMENTAL OBSERVATIONS — CONCLUSIONS

The two basic experimental observations related to the Auger process are shown in Figs. 6 of Ref. 7 and 4 of Ref. 9. Figure 6 of Ref. 7 shows the total decay rate per particle of the ortho excitons as function of the ortho-exciton density. As seen from this graph, the total decay rate is approximately proportional (the exact power is 0.8) to the ortho-exciton density. In this experiment a mode-locked, cavity dumped Argon-ion laser produces nanojoule pulses with about a 100-ps length. For a photoluminescence time resolution of about 100–300 ps, this excitation pulse is effectively a δ function in time, and the evolution of the system is observed without creation by the laser of further particles. The excitons form on a timescale shorter than the detection limits, within a few nanoseconds. The much weaker radiative efficiency of the para excitons makes it difficult to observe them during this short time period. As mentioned earlier, this experiment shows quantum saturation of the ortho excitons, i.e., they move along an adiabat ($-\mu_o/k_B T \approx 0.2$, where μ_o is the chemical potential of the ortho excitons) very close to the condensation line, without condensing; along adiabats $n_o \sim T^{3/2}$. Our result, Eq. (61), gives an approximate linear dependence of the Auger decay rate per ortho exciton as function of the ortho-exciton density. Experimentally the Auger decay rate cannot be measured directly, since ortho-para interconversion⁸ contributes almost as much as the Auger to the total rate shown in Fig. 6 of Ref. 7. Since the decay rate due to the conversion of ortho excitons to para excitons is approximately $\sim T^{3/2}$, which is $\sim n_o$ along an adiabat, the contribution of the Auger decay rate to the total rate experimentally is also $\sim n_o$, in accordance with our theoretical calculation. In the numerical simulation in Ref. 2, the value of 0.40 ns^{-1} for the Auger decay constant C_A (with the density measured in units of 10^{18} cm^{-3}) reproduces the experimental results; this value should be compared with 0.8 ns^{-1} from Eq. (55).

If the mode locker is removed from the laser, the cavity-dumped mode provides 10-ns long pulses with about an order of magnitude more energy. Figure 4(a) of Ref. 9 shows data from lightly stressed crystals with such a long-pulse excitation. The laser profile (triangles), the number of ortho excitons in the lowest ortho-exciton level (open circles), and the number of para excitons (black dots) are shown as function of time in this figure. The stress splits the triply degenerate ortho-exciton level into three components and only the lowest of the three is significantly populated, leading to a closer proximity to the condensation line than in the unstressed case. No ortho-exciton condensation is observed. Under these conditions the para-exciton density was determined from the relative intensities of ortho and para excitons, combined with the spectroscopically determined density of the ortho excitons. This analysis yields the striking evidence that the para excitons condense as shown in Fig. 4(b) of Ref. 9, a graph of the corresponding trajectories for the ortho excitons (open circles) and the para excitons (black dots) in the density-temperature plane. The straight line here is the condensation phase boundary, which is identical for para excitons and ortho excitons in the stressed case. The para excitons in this case are Bose condensed for times later than 8 ns. A crucial feature of the para excitons in these data

which is related with the Auger process is their significantly smaller decay rate than that of the ortho excitons. More specifically, their lifetime is on the order of 100 ns at a density 10^{19} cm^{-3} , while the lifetime of the noncondensed ortho excitons ($\approx 0.1 \text{ nsec}$) is consistent with the phonon-assisted Auger and ortho-para conversion mechanisms discussed earlier, in the case of short-pulse excitation. The para-exciton decay time of 100 ns refers to late times, when the production of excitons due to the laser is negligible, the ortho-exciton density is very low, and essentially only para excitons exist. This observation shows that para-para Auger collisions lead to a very low decay rate. As we showed in Sec. IV, the reason for this low rate is that the band with the required symmetry which assists the para-para phonon-assisted Auger processes is a deep valence band. See Fig. 5. In contrast, for ortho-ortho, or ortho-para collisions the relevant band is very close to the conduction band. In the numerical simulation in Ref. 2 of the time dependence of excitons, we have shown that the ortho excitons move along the phase boundary without crossing it, while the para excitons condense, as a result of the Auger heating of the ortho excitons and phonon cooling of both the ortho and para excitons.

The result of high uniaxial stress $\approx 3.6 \text{ kbar}$ on the Auger process has been resolved in Ref. 10. For comparison, in the data of Fig. 4 of Ref. 9 the stress is $\approx 0.36 \text{ kbar}$; in the data of Fig. 6 of Ref. 7 there is no applied stress. The experiment in Ref. 10 shows clearly that para-para Auger collisions are allowed in stressed crystals. In this experiment laser light produces the excitons away from the well, which drift a distance of $\approx 400 \mu\text{m}$ in the stress gradient to the shear-stress maximum where they are confined. The number of ortho excitons in the well should be negligible, since the relatively short lifetime of ortho excitons precludes travel over $400 \mu\text{m}$ distances; also the expected number of ortho excitons due to thermal excitations is negligibly small under the specific experimental conditions ($T \approx 2 \text{ K}$). Experimentally, however, the measured number of ortho excitons is approximately proportional to the square of the para-exciton number, and the maximum para-exciton density goes as the square root of the laser power. These observations have been attributed to the Auger decay of para excitons.¹⁰ In this case that the crystal is highly stressed, the symmetry selection rules we have used in both the phonon-assisted, as well as the direct processes are expected to break down. An example of this symmetry breaking is that the (zero stress-forbidden) direct recombination line of para excitons has been observed

clearly in stressed crystals; as far as we know, however, the result of stress on phonon-assisted recombination has not been investigated yet.

Stress strongly influences the Auger process, starting with the phonon-assisted mechanism; both the dominant phonon-assisted Auger process involving the Γ_{12}^- phonon as well as the direct Auger become allowed for para-para collisions in stressed crystals, for specific directions of the stress. More specifically, group theory predicts²² that if the uniaxial stress is along the C_2 or the C_3 crystallographic axes, the mixing of the Γ_7^+ with the Γ_8^+ band allows the Γ_{12}^- LO phonon to assist the process. In the specific experiment of Ref. 10 the applied stress is primarily along the C_4 axis, but it also has a component in the C_2 direction. Moreover, uniaxial stress makes the direct Auger process (dominated by the processes shown in diagrams A and A') weakly allowed. Both processes are responsible for the presence of ortho excitons in the quantum well, which are generated by the reformation of Auger-ionized para excitons in random angular momentum states. In both cases the orientation of the uniaxial stress is very important, since it determines the selection rules in the deformed crystal.²²

In summary, we have calculated the direct and phonon-assisted Auger decay rate, incorporating the band structure of Cu_2O , which plays an essential role because of the following effects: (1) the same (positive) parity of the two bands, (2) the fact that the valence band is not a pure spin state, and (3) the symmetry and the location of the negative-parity bands with respect to the conduction and valence bands which form the yellow excitons. The inverse Auger decay times for the direct as well as the much faster phonon-assisted Auger mechanism are proportional to the exciton density. Finally, we have shown that the para-exciton recombination vertex is either forbidden (direct processes), or negligible (phonon-assisted processes), and consequently para-para Auger collisions have a negligible Auger decay rate in nonstressed crystals.

ACKNOWLEDGMENTS

This work was supported by NSF Grants Nos. DMR91-22385 and PHY94-21309. Helpful comments from Y.C. Chang, K. O'Hara, L. O'Suilleabhain, D.W. Snoke, and J.P. Wolfe are gratefully acknowledged. G.M.K. wishes to thank the Research Center of Crete, Greece for its hospitality.

¹D.W. Snoke, J.P. Wolfe, and A. Mysyrowicz, Phys. Rev. Lett. **59**, 827 (1987).

²G.M. Kavoulakis, G. Baym, and J.P. Wolfe, Phys. Rev. B **53**, 7227 (1996).

³A.R. Beattie and P.T. Landsberg, Proc. R. Soc. London Ser. A **249**, 16 (1958); B.K. Ridley, in *Quantum Processes in Semiconductors* (Clarendon, Oxford, 1982); A. Haug, Solid State Commun. **22**, 537 (1977); A. Das and R. Al-Jishi, Phys. Lett. A **141**, 186 (1989); A. Haug, Solid State Electron. **21**, 128 (1978).

⁴P.L. Gourley and J.P. Wolfe, Phys. Rev. B **24**, 5970 (1981); H.

Yoshida, H. Saito, and S. Shionoya, Phys. Status Solidi B **104**, 331 (1981).

⁵V.A. Kiselev and A.G. Zhilich, Fiz. Tverd. Tela **13**, 2398 (1971) [Sov. Phys. Solid State **13**, 2008 (1972)]; M.M. Denisov and V.P. Makarov, Phys. Status Solidi B **56**, 9 (1973); V.P. Makarov, Zh. Éksp. Teor. Fiz. **54**, 324 (1968) [Sov. Phys. JETP **27**, 173 (1968)]; G.E. Pikus and G.L. Bir, Zh. Éksp. Teor. Fiz. **60**, 195 (1971) [Sov. Phys. JETP **33**, 108 (1971)].

⁶A. Mysyrowicz, D. Hulin, and C. Benoît à la Guillaume, J. Lumin. **24/25**, 629 (1981).

- ⁷D.W. Snoke and J.P. Wolfe, Phys. Rev. B **42**, 7876 (1990).
- ⁸D.W. Snoke, D.P. Trauernicht, and J.P. Wolfe, Phys. Rev. B **41**, 5266 (1990); F.I. Kreingol'd and V.L. Makarov, Fiz. Tverd. Tela **15**, 1307 (1973) [Sov. Phys. Solid State **15**, 890 (1973)].
- ⁹J.-L. Lin and J.P. Wolfe, Phys. Rev. Lett. **71**, 1222 (1993).
- ¹⁰D.P. Trauernicht, J.P. Wolfe, and A. Mysyrowicz, Phys. Rev. B **34**, 2561 (1986).
- ¹¹P. Nozières and D. Pines, Phys. Rev. **109**, 741 (1958).
- ¹²J.W. Hodby, T.E. Jenkins, C. Schwab, H. Tamura, and D. Trivich, J. Phys. C **9**, 1429 (1976).
- ¹³P.T. Landsberg, in *Recombination in Semiconductors* (Cambridge University Press, New York, 1991).
- ¹⁴A.R. Beattie and P.T. Landsberg, Proc. R. Soc. London Ser. A **258**, 486 (1960); P. Dzwig, J. Phys. C **12**, 1809 (1979).
- ¹⁵J.P. Dahl and A.C. Switendick, J. Phys. Chem. Solids **27**, 931 (1965); R. J. Elliott, Phys. Rev. **124**, 340 (1961); L. Kleinman and K. Mednick, Phys. Rev. B **21**, 1549 (1980).
- ¹⁶E.O. Kane, in *Physics of III-IV Compounds*, edited by R.K. Willardson and A.C. Beer, Semiconductors and Semimetals Vol. 1 (Academic, New York, 1966), p. 75.
- ¹⁷G.M. Kavoulakis, Yia-Chung Chang, and Gordon Baym (unpublished).
- ¹⁸S. Nikitine, J.B. Grun, and M. Sieskind, J. Phys. Chem. Solids **17**, 292 (1961).
- ¹⁹R.J. Elliott, Phys. Rev. **108**, 1384 (1957); S. Nikitine, in *Optical Properties of Solids*, edited by S. Nudelman and S.S. Mitra (Plenum, New York, 1969), p. 127.
- ²⁰A.F. Gross and A.A. Kaplyanskii, Fiz. Tverd. Tela **2**, 379 (1960) [Sov. Phys. Solid State **2**, 353 (1960)].
- ²¹A. Mysyrowicz, D. Hulin, and A. Antonetti, Phys. Rev. Lett. **43**, 1123 (1979).
- ²²A. Mysyrowicz, D.P. Trauernicht, J.P. Wolfe, and H.-R. Trebin, Phys. Rev. B **27**, 2562 (1983); F.I. Kreingol'd and V.L. Makarov, Fiz. Tekh. Poluprovodn. **8**, 1475 (1974) [Sov. Phys. Semicond. **8**, 962 (1975)]; H.-R. Trebin, H.Z. Cummins, and J.L. Birman, Phys. Rev. B **23**, 597 (1981); S.A. Moskalenko and A.I. Bobrysheva, Fiz. Tverd. Tela **4**, 1994 (1962) [Sov. Phys. Solid State **4**, 1462 (1963)].
- ²³Ch. Uihlein, D. Fröhlich, and R. Kenklies, Phys. Rev. B **23**, 2731 (1981).
- ²⁴P.D. Bloch and C. Schwab, Phys. Rev. Lett. **41**, 514 (1978); J.L. Birman, Solid State Commun. **13**, 1189 (1973).